

# Upper limits to surface force disturbances on LISA proof-masses and the possibility of observing galactic binaries

L. Carbone,<sup>1</sup> A. Cavalleri,<sup>2</sup> G. Ciani,<sup>1</sup> R. Dolesi,<sup>1</sup> M. Hueller,<sup>1</sup> D. Tombolato,<sup>1</sup> S. Vitale,<sup>1</sup> and W. J. Weber<sup>1</sup>

<sup>1</sup>*Department of Physics, University of Trento and INFN, Gruppo Collegato di Trento, I-38050, Povo, Trento, Italy*

<sup>2</sup>*Istituto di Fotonica e Nanotecnologie CNR-ITC and INFN Gruppo Collegato di Trento, I-38050 Povo, Trento, Italy*

We report on the measurement of parasitic surface force noise on a hollow replica of a LISA (Laser Interferometer Space Antenna for the observation of gravitational waves) proof-mass (PM) surrounded by a faithful representation of its in-flight surroundings, namely the capacitive sensor used to detect PM motion. Parasitic forces are detected through the corresponding torque exerted on the PM and measured with a torsion pendulum in the frequency range  $0.1 \div 30$  mHz. The sensor electrodes, electrode housing and associated readout electronics have the same nominal design as for the flight hardware, including 4 mm gaps around the PM along the sensitive laser interferometry axis. We show that the measured upper limit for surface forces would allow detection of a number of galactic binaries signals with signal to noise ratio up to  $\approx 40$  for 1 year integration. We also discuss how the flight test under development, LISA Pathfinder, will substantially improve this limit, approaching the performance required for LISA.

**Introduction.** LISA is a space-borne gravitational wave detector under development by the American (NASA) and European (ESA) space agencies [1]. The detector measures, by means of a laser interferometer, the gravitational wave-induced change in the distance between free-falling proof-masses (PMs) separated by  $\approx 5 \times 10^9$  m. Three PM pairs define three lines that form a nearly equilateral triangle. The PM pairs are assumed to be in pure geodesic motion, free of spurious *relative* acceleration noise along the measurement axis (referred to as  $x$  from now on) to within  $\sqrt{2} \times \{3 \times 10^{-15} (\text{m/s}^2 \sqrt{\text{Hz}}) (1 + (f/3\text{mHz})^4)^{1/2}\}$ , where  $f$  is the frequency.

The PMs in LISA are cubes made of a Au-coated Au-Pt alloy and as such are solid conducting bodies with no mechanical contact to the surroundings. The relevant disturbing forces can be divided into forces into those that act on the surface, which are most significant, and those acting on the bulk, namely low frequency magnetic and gravitational effects. Both the magnetic fields generated inside the spacecraft (SC) and the PM magnetic properties can be measured on ground with sufficient accuracy, and thus the resulting magnetic force noise expected in flight can be well characterized. The interplanetary magnetic field is known to be stable enough to be a minor entry in the LISA error budget [2]. As there are no continuously moving masses in the current LISA design, the most worrisome gravitational noise source is the SC thermo-mechanical distortion. Were this distortion known in detail, the gravitational noise on the PM would then be well modeled based on the measured mass properties. Modeling of thermo-mechanical distortion is part of the LISA Pathfinder mission [3], the LISA precursor under development by ESA, as is an in-flight measurement.

Surface forces include, among other disturbances, low frequency electric field fluctuations, back-action from the electrostatic position readout, thermal radiation effects, and residual pressure gradients. These forces are the

most difficult to model, as they may be connected, for instance, to electrochemical or radiative properties of the PM and electrode surfaces.

In LISA the PM is surrounded by a system of electrodes used to detect the PM motion within the SC. 6 pairs of electrodes are used to sense the proof mass motion in all degrees of freedom, using 100 kHz capacitance bridge readouts. In addition a set of biasing electrodes on opposing faces along one or both directions normal to  $x$  provides the PM ac-voltage polarization required by the bridge to work. The position information is fed back to control loops that suppress relative SC-PM motion. We call this electrode system, together with its support housing, the necessary readout coaxial cables, and other accessories, the Gravity Reference Sensor (GRS). The GRS creates a nearly closed cavity around the PM, and, with its Au-coated electrodes and housing, serves as an electrostatic shield. Thus the GRS shields the PM from external sources of surface force and is, in practice, the dominant source of surface force disturbances.

We proposed [4] a torsion pendulum to investigate surface forces on LISA-like PMs. A first measurement campaign [5] employed a prototype sensor with a hollow, 40 mm Au-coated Ti PM, suspended in-axis with a W wire, with 2 mm gaps to the surrounding sensor electrode surfaces. The hollow PM allows use of a thinner torsion fiber, and thus higher force sensitivity, than with the full 2 kg LISA PM, without sacrificing representativity for surface forces [4, 5]. The electrodes were Au-coated Mo plates, with biasing electrodes only along one axis (the  $z$ -axis). A simple home-made sensor readout electronics was used for the measurements.

In connection with the implementation of the LISA Pathfinder mission [3], the design of the GRS has evolved [6]. The PM is now a 46 mm cube, separated from the electrodes by a gap of 4 mm along the  $x$ -direction, and 2.9 mm and 3.5 mm on the other axes. The electrodes are now Au-coated ceramic pieces mounted inside a Mo

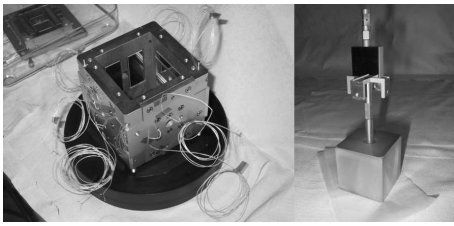


FIG. 1: Left: the electrode housing of the GRS used for the reported measurements. The AU-coated ceramics electrodes for the x-direction motion readout are the pair of shiny vertical plates visible inside the sensor. Also visible, on the adjacent y face, is a y-sensing electrode, the upper horizontal plate, and one of the electrodes used to polarize the PM for capacitive readout (with a circular hole in the center). Right: the hollow PM used for the torque measurements.

structure. In addition the biasing electrodes are present on all faces except the ones along  $x$ .

In this article we describe the results of a measurement campaign performed with the torsion pendulum on a prototype of this new sensor design, connected to a readout electronics closely following the final flight-hardware design. From the results we derive an upper limit for surface forces on the PM for LISA. Finally, we briefly compare this performance with that expected from LISA Pathfinder for the entire force disturbance budget.

The main features of the prototype are described above, with a photograph shown in Fig.1. Details of the readout scheme can be found both in [5, 6]. Also shown in Fig.1 is the pendulum inertial element, featuring a 46 mm hollow Al cube suspended by a W wire by means of an Al shaft. The shaft is electrically isolated from the PM via a quartz ring hidden underneath the top face of the PM. A mirror used for the independent optical readout of the angular motion is attached to the shaft, along with a structure used to balance the entire setup. The total moment of inertia  $I_o = (4.31 \pm 0.01) \times 10^{-5}$  kg m<sup>2</sup>. The PM is suspended under high vacuum ( $10^{-5}$  Pa). The resulting torsional oscillator has a period approximately  $T_o = 564$  s, the exact value depending on the applied electrical field, and a quality factor  $Q = 2900 \pm 500$ .

The GRS is mounted on a micro-manipulator that allows moving and centering it around the PM, to which it has no mechanical contact. This manipulator, together with an additional one at the upper pendulum suspension point, allows the centering in all degrees of freedom with  $\mu\text{m}$  precision. The pendulum motion is measured both by the GRS and by an independent optical readout based on a commercial autocollimator. The GRS has a sensitivity of order  $2 \text{ nm}/\sqrt{\text{Hz}}$  in displacement and  $200 \text{ nrad}/\sqrt{\text{Hz}}$  in rotation down to frequencies of 1 mHz, with no reliable measurement below this frequency. It provides the PM motion readout in all 6 degrees of freedom. The autocollimator has an intrinsic resolution of  $20 \text{ nrad}/\sqrt{\text{Hz}}$  within the same frequency

range and provides the readout for both the torsion angle and pendulum tilt around one horizontal axis. The GRS is equipped with heaters and thermometers, while optical fibers can shine UV light on PM or electrode housing to discharge the PM. A 3-axis magnetometer monitors the low frequency magnetic field fluctuations with a resolution of  $1 \text{ pT}/\sqrt{\text{Hz}}$  above 1 mHz and a  $1/f$  upturn below this frequency. More details on the pendulum can be found in [4, 5].

The angular motion of the pendulum  $\phi(t)$  is converted into an instantaneous external applied torque  $N(t)$  as

$$N(t) = I_o \left\{ \ddot{\phi}(t) + \frac{2\pi}{T_o Q} \dot{\phi}(t) + \left( \frac{2\pi}{T_o} \right)^2 \phi(t) \right\} \quad (1)$$

In practice, the derivatives are estimated from a sliding second order fit to 5 adjoining data. Eq.(1) approximates the damping as viscous, while in reality it is dominated by structural dissipation within the fiber. However, the difference between these two models has no detectable effect on data processing.

In order to get an estimate of the expected readout background noise, we formed the average,  $\bar{N}(t) = [N_{GRS}(t) + N_{ac}(t)]/2$ , and semi-difference,  $\delta N(t) = [N_{GRS}(t) - N_{ac}(t)]/2$  of the torques,  $N_{GRS}(t)$  and  $N_{ac}(t)$ , calculated, respectively, from the GRS and autocollimator angular readouts  $\phi_{GRS}(t)$  and  $\phi_{ac}(t)$ . For ideally uncorrelated readout noise, the power spectral densities (PSD) of these signals should be:

$$S_{\bar{N}}(f) = S_N(f) + \frac{S_{n,\phi_{GRS}}(f) + S_{n,\phi_{ac}}(f)}{4|H(f)|^2} \quad (2)$$

$$S_{\delta N}(f) = \frac{S_{n,\phi_{GRS}}(f) + S_{n,\phi_{ac}}(f)}{4|H(f)|^2} \quad (3)$$

where  $S_X(f)$  is the PSD of process  $X$  at frequency  $f$ ,  $S_{n,\phi_{GRS}}(f)$  and  $S_{n,\phi_{ac}}(f)$  are the PSDs of the uncorrelated angular readout noise of, respectively, the GRS and autocollimator, and  $H(f) = \{I_o(2\pi)^2[(1/T_o)^2 - f^2 + i(f/T_o Q)]\}^{-1}$  is the pendulum torque-to-angle transfer function. Thus within this model one can estimate the torque PSD by:

$$S_N(f) = S_{\bar{N}}(f) - S_{\delta N}(f) = \text{Re} \{S_{N_{ac}, N_{GRS}}(f)\} \quad (4)$$

Eq.(4) indicates that in this model the difference  $S_{\bar{N}}(f) - S_{\delta N}(f)$ , attributed to true torque noise measured above the readout limit, is equivalent to the correlated noise between the two readout signals, and can be calculated as the cross-power spectral density (CSD)  $\text{Re} \{S_{N_{ac}, N_{GRS}}(f)\}$  between  $N_{GRS}(t)$  and  $N_{ac}(t)$ . Note that, in the absence of a definite excess torque, the result of this estimate, if calculated as a PSD difference or CSD, can give negative values due to statistical fluctuations.

PSD and cross-spectral densities are estimated by standard Welch periodogram, using a Blackman-Harris  $3^{\text{rd}}$

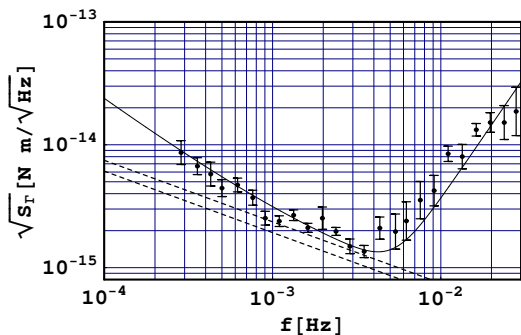


FIG. 2: Total torque noise. Data points: square root of torque noise PSD estimated from autocollimator and capacitive sensor cross-correlation after time domain subtraction of the effect of PM motion along  $y$ . Values and error bars are estimated as the mean and its standard deviation of PSD data falling within the corresponding frequency bins. Bins have equal logarithmic width. Dashed lines delimit the error band for the estimate of thermal noise. The continuous smooth line is a linear least square fit to data as described in the text.

order window and by averaging over 20 data segments, adjoining data segments overlapping by 50%. Data segments are individually de-trended by subtracting the best fit straight line to the data. The accuracy of the method has been tested with a variety of simulated data. Simulation shows that in the presence of large drift or in general substantial noise power below the measurement bandwidth, the two lowest frequency points follow the frequency shape of the side lobes of the spectral window. These points are then discarded during further data processing. In Fig.2 we report an example of the outcome of this data reduction procedure.

In this specific run, following an air re-entry into the vacuum chamber, an extra coupling to motion of PM in the  $y$ -direction was detected.  $\bar{N}(t)$  data consequently showed a very strong correlation with this motion as measured by the GRS. This motion is a few orders of magnitudes larger than any SC motion relevant for LISA, and thus a small coupling may convert into a large torque that would not translate into a corresponding force on a LISA PM. We thus subtracted the  $y$ -signal of the GRS multiplied just by a constant from the  $\bar{N}(t)$  data series. The constant was chosen by minimizing the residual noise at low frequency and was found to be  $\partial\Gamma/\partial y = (-9.8 \pm 2.2)$  nN. This number, confirmed in other runs, agrees with the results of coarse measurement obtained by moving the GRS with the micromanipulator that gives  $\partial\Gamma/\partial y \approx 7$  nN. Coincident with the appearance of this extra coupling, additional angular stiffness was detected, measured by rotating the GRS [8]. This extra angular stiffness amounts to  $\partial^2\Gamma/\partial\phi^2 = (1.43 \pm 0.02) \times 10^{-10}$  Nm/rad. The data for  $\partial\Gamma/\partial y$  and for  $\partial^2\Gamma/\partial\phi^2$  taken together, suggest a localized charged feature on the  $y$ -face at  $\approx 1.5$  cm from

TABLE I: Results of the estimate of excess noise coefficients.

Prototype	$f^{-2}$ coeff. [ $\text{N}^2\text{m}^2\text{Hz}$ ]	$f^4$ coeff. [ $\text{N}^2\text{m}^2\text{Hz}^{-5}$ ]
46 mm PM 4 mm gap	$(3.7 \pm 0.3) \times 10^{-36}$	$(3.8 \pm 0.4) \times 10^{-21}$
40 mm PM 2 mm gap	$(5.0 \pm 0.4) \times 10^{-36}$	$(1.3 \pm 0.2) \times 10^{-21}$

the center, compatible with the observed slow decay of the effect with time. We suspect that such a charge is due to one of many observed defects in the electrode Au-coating that expose the potentially-charged dielectric underneath. The overall effect of subtraction is to decrease the noise by a factor 2 between 0.2 mHz and  $\approx 2$  mHz, with negligible effect at higher frequencies.

The figure also shows the expected contribution from the thermal torque noise associated with pendulum damping and providing the ultimate torque noise floor. As damping at these low frequencies is dominated by dissipation within the fiber, thermal noise is expected to have a PSD

$$S_{th}(f) = 4k_B T \frac{I_o (2\pi/T_o)^2}{2\pi f Q} \quad (5)$$

with  $T$  the temperature and  $k_B$  the Boltzmann constant.

The figure shows that even after subtraction of the effect of motion along  $y$ , residual noise coincides with the expected thermal background, within the errors, only near 1-2 mHz. In order to quantify the extra noise at other frequencies we performed a fit to the excess with a simple polynomial law of frequency in the range  $0.2 \div 30$  mHz by a weighted least square procedure. Many different power laws were tested with linear combinations of both positives and negative exponents. The only choice giving fully significant F-test value for all terms in the polynomial is the superposition of a  $1/f^2$  law with a term proportional to  $f^4$ . This is true for all other experimental runs we have investigated (see below). The results of the fitting are reported in Fig.2. Coefficients and uncertainties are reported in Tab.(I). The same table reports the results for a run performed with the 40 mm PM, 2 mm gaps prototype. Both runs were performed with same W torsion fiber.

**Discussion.** Fig.2 shows that excess noise only becomes negligible around 2-3 mHz. Below this frequency the  $1/f^2$  term is a significant contribution to the noise that brings total noise to a value which is 40% above the background at 1 mHz and 2 times this one at 0.2 mHz. We have not yet understood the origin of this excess. There is no significant correlation with the magnetometer readout. A weak, barely significant correlation between  $\bar{N}(t)$  and the thermometer monitoring the vacuum column enclosing the torsion fiber was found. This temperature was also correlated with the vertical motion  $z(t)$  of the PM that consequently showed a correlation with

$\bar{N}(t)$ . A subtraction of this effect would lower the excess by only 10% .

A few considerations seem to indicate that the excess is a property of the pendulum and is not connected to the interaction between the PM and GRS. First the noise level has not been significantly affected by the change in the design of the GRS (Tab.(I)), with the difference between the results obtained with the two prototypes being well within the variability, of a factor  $\approx 2$ , observed for each prototype among different runs taken at different times during the many-month campaigns performed in each case. This is true even though changing 2 mm to 4 mm gaps represents a major change, significantly reducing, for instance, the coupling between charge patches [7] and significantly increasing the gas molecular conduction around the PM.

A candidate source for the measured torque excess is connected with the continuous unwinding of the fiber due to creep in the fiber material. In the runs presented, the fiber unwound with a rate of  $\approx 2 \times 10^{-10}$  rad/s. The rate is reduced by temperature annealing the fiber under load. Unfortunately we are limited by practical reasons to an annealing temperature of only  $\approx 60^\circ\text{C}$ . It is interesting to note that a simple Poisson model where single angular slip events of amplitude  $\delta\phi$  contribute to both unwinding and the residual noise, yields a step size of  $\delta\phi \approx 40$  nrad and a rate of  $\approx 510^{-3} \text{ s}^{-1}$ .

We searched for evidence of such glitches by running a Wiener-Kolmogorov filter on the data matched to step-shaped torque signals. The filter resolution for angular steps, resulted to be  $\sigma = 33$  nrad, roughly the size expected from the reasoning above. The filter did indeed detect several well identified large amplitude ( $3 - 5\sigma$ ) events, satisfying goodness-of-the-fit test criteria, and which accounted for  $\approx 20\%$  of the excess noise at low frequency.

One can even entirely suppress the excess noise at low frequency by subtracting the  $\approx 200$  highest events, with amplitude as low as  $\pm 2\sigma$ . However, while these results can be taken as an indication of angular glitches as the possible source for the detected excess noise at low frequency, they cannot be considered as an unambiguous proof and such events have not been subtracted from the data of Fig.2. It is worth remembering that any data series can be approximated with arbitrary precision by a sequence of variable amplitude steps and thus a subtraction procedure can possibly, and erroneously, cancel the noise entirely.

The high frequency excess proportional to  $f^4$  is also statistically significant. The excess is due to a residual correlation between the readouts at high frequency. The real part of cross-coherence  $r(f) = \text{Re}(S_{\phi_{ac}, \phi_{GRS}}(f)) / \sqrt{S_{\phi_N}(f) S_{\phi_r}(f)}$ , is still  $0.10 \pm 0.02$  at 10 mHz, dropping to non-significant values only above 60 mHz.

It would be truly difficult to attribute this excess to any

real torque on the PM. For instance, when converted to a voltage on one of the electrodes, this would amount to a PSD of  $4 \text{ V}/\sqrt{\text{Hz}}$  at 300 mHz assuming an unrealistically large dc voltage of 2 V on the same electrode, all figures unlikely by orders of magnitude [8].

The  $f^4$  dependence converts into a white rotational noise of the entire apparatus relative to the local frame of inertia by  $\approx 30 \text{ nrad}/\sqrt{\text{Hz}}$ . Thus a possible explanation may be such a rotation due either to seismic noise or to local mechanical distortion. However a residual electrical cross-talk between GRS and autocollimator cannot be excluded.

Though the detected excess is likely not due to the GRS itself and is not then relevant to LISA, we still include it when the estimating the upper limit to the disturbances acting on the PM. This upper limit also includes the fit uncertainty and by the uncertainty in the evaluation of thermal noise, conservatively estimated to be 20% and coming from the error in Q-factor measurement.

Overall this upper limit for the data of Fig.2, defining  $f_o = 1 \text{ mHz}$  is:

$$3 \cdot 10^{-30} \frac{\text{N}^2 \text{m}^2}{\text{Hz}} \left\{ 1.2 \left( \frac{f_o}{f} \right)^2 + 0.3 \left( \frac{f_o}{f} \right) + 1.2 \cdot 10^{-3} \left( \frac{f}{f_o} \right)^4 + \sqrt{10^{-2} \left( \frac{f_o}{f} \right)^4 + 2.2 \cdot 10^{-8} \left( \frac{f}{f_o} \right)^8} \right\}$$

These torque data can be converted into an equivalent acceleration noise with a few simple assumptions on the contributing effects [5]. For instance simulations [5] give that randomly distributed normal forces, like those associated with parasitic electric fields, would exert both torque and force noise, with a ratio of their amplitudes of roughly  $0.4L$ , with  $L$  the PM size. This holds for disturbances with spatial exponential correlation lengths up to  $L/10$ . The ratio would decay to  $L/4$  for a correlation slightly larger than  $L$ .  $L/4$  is also roughly the ratio obtained for an electrical disturbance directly applied to the electrodes of the  $x$ -face, as would be expected from electronic readout back-action. Finally forces acting tangentially, like diffuse scattering of molecules, show a ratio of  $L/2$ . We then convert the torque to an equivalent acceleration noise that the corresponding forces would exert on the 1.96 kg LISA PM by using the lowest ratio  $L/4$ , i.e. 10.7 cm. The reader should be aware though that obviously our pendulum geometry would not detect disturbances applied uniformly and normal across the  $x$  face or tangentially to the  $y$  and  $z$  faces, or disturbances acting normally onto the center of the  $x$ -face or in a few other symmetric positions.

The results of the conversion of the data of Fig.2 into an equivalent acceleration noise are reported in Fig.3. Within the same figure we also report for comparison the acceleration level that would guarantee to LISA a measurement of the gravitational wave signal from a few binary systems in our Galaxy over one year integration

